AD_____

Award Number: DAMD17-00-1-0459

TITLE: Non-Invasive Monitoring of Breast Tumor Oxygenation: A Key to Tumor Therapy Planning and Tumor Prognosis

PRINCIPAL INVESTIGATOR: Hanli Liu, Ph.D.

CONTRACTING ORGANIZATION: The University of Texas at Arlington
Arlington, Texas 76019-0145

REPORT DATE: September 2001

TYPE OF REPORT: Annual

PREPARED FOR: U.S. Army Medical Research and Materiel Command
Fort Detrick, Maryland 21702-5012

REPORT DOCUMENTATION PAGE

Form Approved
OMB No. 074-0188

1. AGENCY USE ONLY (Leave blank)	2. REPORT DATE	3. REPORT TYPE AND DATES COVERED
	September 2001	Annual (1 Sep 00 - 31 Aug 01)

4. TITLE AND SUBTITLE
Non-Invasive Monitoring of Breast Tumor Oxygenation: A Key to Tumor Therapy Planning and Tumor Prognosis

5. FUNDING NUMBERS
DAMD17-00-1-0459

6. AUTHOR(S)
Hanli Liu, Ph.D.

7. PERFORMING ORGANIZATION NAME(S) AND ADDRESS(ES)
The University of Texas at Arlington
Arlington, Texas 76019-0145

E-Mail: hanli@uta.edu

8. PERFORMING ORGANIZATION REPORT NUMBER

9. SPONSORING / MONITORING AGENCY NAME(S) AND ADDRESS(ES)
U.S. Army Medical Research and Materiel Command
Fort Detrick, Maryland 21702-5012

10. SPONSORING / MONITORING AGENCY REPORT NUMBER

11. SUPPLEMENTARY NOTES

12a. DISTRIBUTION / AVAILABILITY STATEMENT
Approved for Public Release; Distribution Unlimited

12b. DISTRIBUTION CODE

13. ABSTRACT *(Maximum 200 Words)*

The goal of this research project is to develop and evaluate a new approach to monitoring of vascular hemoglobin oxygen saturation (SO_2) and oxygenated hemoglobin (HbO_2) concentration of breast tumors using near infrared (NIR) spectroscopy and imaging techniques. We have evaluated a single-channel, dual wavelengths, NIR, frequency-domain oximeter and the corresponding algorithm for obtaining tumor SO_2 and HbO_2 under carbogen intervention against tumor pO_2 measurement using NIRS and needle type pO_2 electrodes, and the pO_2 data were supported by the ^{19}F MR pO_2 mapping. The NIRS data showed significant changes in vascular oxygenation accompanying respiratory interventions, and changes in tumor vascular hemoglobin oxygenation preceded tumor tissue pO_2. A combined algorithm has been developed for quantifying absolute deoxygenated Hb, oxygenated Hb, and total Hb concentrations, and this algorithm is particularly developed for our single source-detector separation, two wavelengths, NIR, frequency-domain system. With this algorithm, we are able to obtain relatively accurate results of total Hb concentrations with possible scattering variations.

14. SUBJECT TERMS
Technology Development, Radiologic Sciences, Tumor Therapy Planning and Prognosis, Tumor Physiology Monitoring

15. NUMBER OF PAGES
48

16. PRICE CODE

17. SECURITY CLASSIFICATION OF REPORT	18. SECURITY CLASSIFICATION OF THIS PAGE	19. SECURITY CLASSIFICATION OF ABSTRACT	20. LIMITATION OF ABSTRACT
Unclassified	Unclassified	Unclassified	Unlimited

Table of Contents

2000-2001 ANNUAL PROGRESS REPORT (YEAR 1)

This report presents the specific aims and accomplishments of our breast cancer research project during the first year of funding sponsored by the U.S. Department of the Army. It covers our activities from September 1, 2000 to October 31, 2001.

Introduction

The goal of this research project is to develop and evaluate a new approach to monitoring of vascular blood oxygen saturation (SO_2) and blood concentration (Hb) of breast tumors using near infrared (NIR) spectroscopy and imaging techniques. Further, we wish to compare and validate the optical method with concurrent measurements of tumor oxygen tension on the basis of ^{19}F EPI relaxation of hexafluorobenzene (HFB). Once we have rigorously established the integrated approach to tumor physiology, we will explore the influence of three interventions expected to modify tumor physiology. A better understanding of the interplay of these parameters in the natural history of a tumor could lead to enhanced therapeutic approaches and provide a novel diagnostic/prognostic tool for breast cancer research and clinical practice.

The project has four specific aims:
Aim 1: To evaluate a single-channel, dual wavelength, NIR, frequency-domain oximeter and the algorithms for obtaining tumor SO_2 against tumor pO_2 measured by ^{19}F EPI relaxation of HFB.
Aim 2: To modify the single-channel system into a 3-channel NIR system.
Aim 3: To investigate heterogeneity of SO_2 in breast tumors using the 3-channel NIR system.
Aim 4: To study the influence of three interventions on SO_2 and pO_2 of the tumor simultaneously.

Specifically, Task 1 was planned for months 1-15 to accomplish Aim 1:
Task 1: To evaluate a single-channel, dual wavelength, NIR, frequency-domain oximeter and the corresponding algorithm for obtaining tumor SO_2 against tumor pO_2 measurement using ^{19}F MR EPI of hexaflourobenzene, ***(months 1-15)***:

a. test and calibrate the existing single-channel, dual wavelength, NIR oximeter using blood-yeast models to achieve a stable and low-noise system;
b. perform laboratory NIR and MR EPI measurements on rat breast tumors under two respiratory conditions (33% oxygen as the base line and 100% as an intervention).
c. employ proper algorithms to calculate absolute values and changes of SO_2 and Hb in the tumor vascular bed before, during, and after the respiratory challenge.
d. Compare the SO_2 values with pO_2 and study vascular and tissue dynamic response to the respiratory change.

Body of the Report

As mentioned in Introduction section, our Year 1 focus was to achieve Task 1, and we have mainly accomplished this task, as reported below:

Task 1a: to test and calibrate the existing single-channel, dual wavelength, NIR oximeter using blood-yeast models to achieve a stable and low-noise system;

The PI and her graduate student, Jae Kim, have made significant efforts to accomplish this task. Two kinds of experiments were performed to calibrate our NIR system: 1) cross-talk

measurement between amplitude and phase of the instrument and 2) blood phantom measurement for error analysis.

Crosstalk Study

In principle, changes in amplitude of a frequency-domain photon migration system are independent of its changes in phase, i.e., the crosstalk between amplitude and phase should be minimal for an ideal NIR system. However, in reality, it is difficult to have such a perfect condition for an actual instrument and necessary to calibrate the system. To conduct the crosstalk test, we altered optical filters in front of the two light sources (758 nm and 785 nm) to attenuate the optical amplitude, so we could see whether phase data were influenced by amplitude changes. The test showed that the phase-amplitude crosstalk exists if the measured output signal is either too large or too small. We concluded that the output range of our instruments should be between 350 mV and 100 mV during measurement (Figs. 1 and 2) to avoid the unwanted phase-amplitude crosstalk.

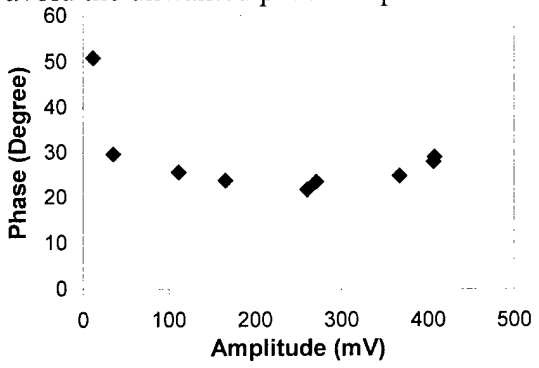

Figure. 1 Crosstalk test for 758nm wavelength

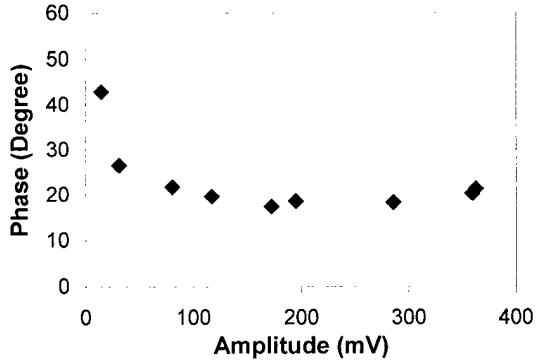

Figure. 2 Crosstalk test for 785nm wavelength

We also plotted O.D (optical density) of the filters versus log(amplitude of the measured output signal) to see the electrical response of the instrument when the input light intensity changes. It was found that as long as we are in the output range of 100 mV to 350 mV, we can achieve good linearity for the system response, as shown in Figures 3 and 4.

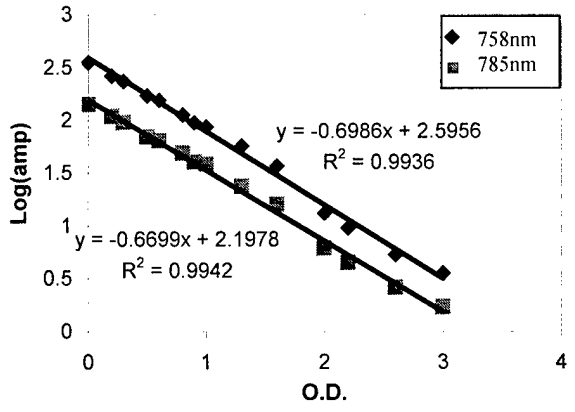

Figure 3. Linear system response between O.D. and Log(amplitude) (starts from 350mV amplitude).

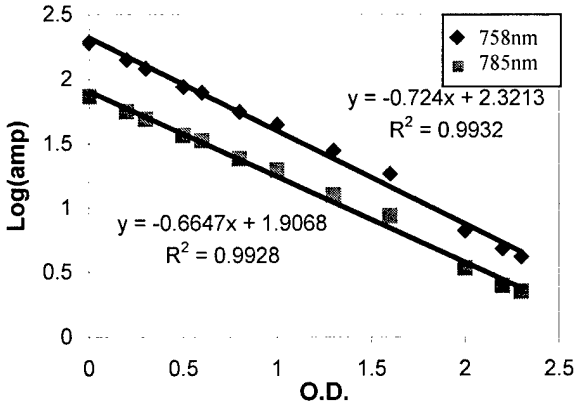

Figure. 4 Linear system response between O.D. and Log(amplitude) (starts from 193mV amplitude).

Blood Phantom Study

To calibrate our NIR system for quantifying hemoglobin concentrations, we used human blood for tissue phantom experiments. The measurements were conducted at the University of Pennsylvania since the graduate student, Jae Kim, needed some training in conducting this kind of experiments. One packet of SIGMA P-3813 phosphate buffered saline (pH 7.4) powder was used to make a 2-litter buffer, and 100 ml of 20% intralipid were added into the buffer for a 1% intralipid solution. Then 14g of baking yeast were mixed with tap water before being added into the 2-litter buffer solution.

Amount of blood for each addition to the solution was 3 ml for the first two additions and 6 ml for later additions. For the first two additions, we added 3 ml of blood each time, which contained 6.6 μmoles of hemoglobin and gave a concentration of 3.3 μM in the solution (= 6.6 μmoles / 2 L). The later 6 ml of blood addition resulted in an addition of 6.6 μM (= 13.2 μmoles/2L) in hemoglobin concentration.

In the NIR range, major light chromophores in tissues are Hb and HbO_2. Therefore, the absorption coefficients at two wavelengths can be associated with the concentrations of Hb and HbO_2, expressed as [Hb] and [HbO_2], respectively, by

$$\mu_a^{758} = \varepsilon_{Hb}^{758}[Hb] + \varepsilon_{HbO2}^{758}[HbO_2], \quad (1)$$
$$\mu_a^{785} = \varepsilon_{Hb}^{785}[Hb] + \varepsilon_{HbO2}^{785}[HbO_2]\ . \quad (2)$$

Our algorithm is based on modified Beer-Lambert's Law, which has the following expression.

$$\ln(I_o/I) = = \mu_a L, \quad (3)$$

where I_o and I are the incident and the detected optical intensities, respectively, and L is the optical path length traveled by light inside the medium.

Therefore, changes of absorption coefficients can be expressed as

$$\Delta\mu_a = \mu_{aT} - \mu_{aB} = \ln(I_o/I_T)L - \ln(I_o/I_B)L = \ln(I_B/I_T) / L, \quad (4)$$

with the assumption that L is constant. Then the changes of Hb and HbO_2 concentrations can be calculated by

$$\Delta[HbO_2] = [-5.73*\ln(I_B/I_T)^{758} + 9.67*\ln(I_B/I_T)^{785}] / L, \quad (5)$$

$$\Delta[Hb]_{total} = \Delta[Hb] + \Delta[HbO_2] = [-1.32*\ln(I_B/I_T)^{758} + 6.23*\ln(I_B/I_T)^{785}] / L, \quad (6)$$

where I_B = baseline amplitude; I_T = transition amplitude; L = optical pathlength between source/detector; the constants were computed with the extinction coefficients for human oxy and deoxyhemoglobin at the two wavelengths used. Some details for the algorithms can be found in the manuscript attached in Appendix a.

By using eqs. (5) and (6), we can obtain $[HbO_2]$ and $[Hb]_{total}$, as plotted in Figure 5. This figure basically shows that 33 μM and 30 μM of $[Hb]_{total}$ increased for the first two additions of 3 ml blood, and 52 μM and 59 μM of $[Hb]_{total}$ increased for the third and fourth 6 ml blood additions. These are about 10 and 8.5 times larger than 3.3 μM and 6.6 μM, respectively. Further studies are being conducted to understand the origin of this large factor.

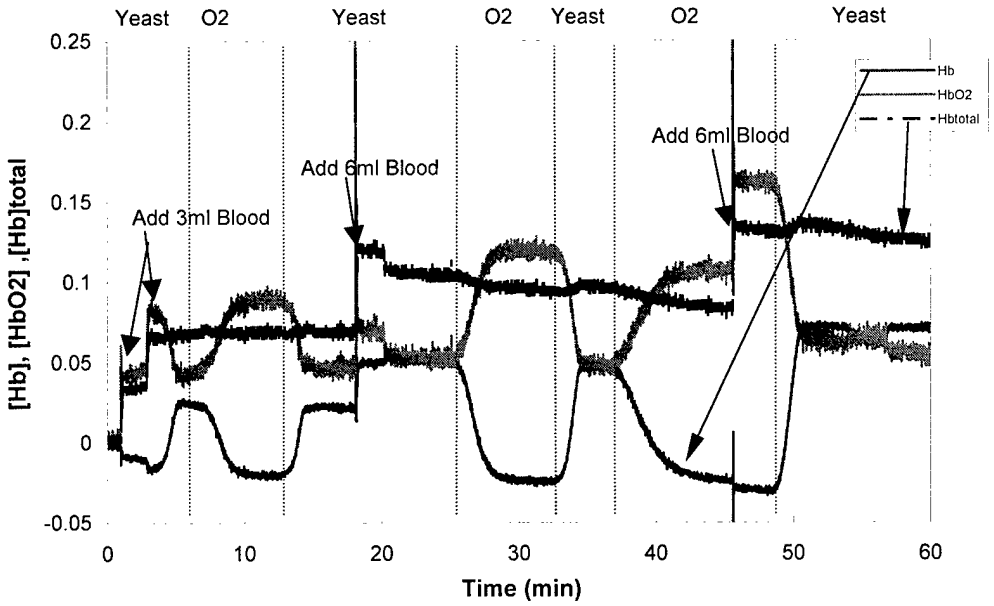

Figure 5. Phantom experiment using 1% intralipid in a saline solution. Changes of [Hb], $[HbO_2]$, $[Hb]_{total}$ during oxygenation and deoxygenation process were measured by using NIRS.

During the studies, we also learned that a small variation in extinction coefficients could cause large variations in determinations of $[HbO_2]$ and $[Hb]_{total}$. Extinction coefficients of human oxy-hemoglobin and deoxy-hemoglobin can be found in two sources given by Zijlstra and Cope[1,2]. Until now we had used Zijlstra's extinction coefficients, but we have found that using Mark Cope's extinction coefficients give us better results of changes in hemoglobin oxygenation. We applied Cope's extinction coefficients in this report. In Mark Cope's dissertation, extinction coefficients of hemoglobin were quoted for a molecular weight of 64450 and hence four times larger than the values that are quoted as "per equivalent". Each hemoglobin molecule consists of four protein chains called *globins*, each of which is bound to one *heme*, a red-pigmented molecule that contains iron. Therefore, to use his extinction coefficients as "per equivalent" we need to divide his extinction coefficient by four.

The changes in total hemoglobin concentration in the blood phantom study showed that Mark Cope's extinction coefficients divided by 4 resulted in the theoretical/expected values when we assumed that the DPF of the phantom solution is about 9 (please refer to the manuscript in Appendix a for DPF). We are continuing to explore the crucial relationship between the extinction coefficients and accurate determinations for $[HbO_2]$ and $[Hb]_{total}$.

Task 1b: to perform laboratory NIR and MR EPI measurements on rat breast tumors under two respiratory conditions (33% or 21% oxygen as the base line and 100% or Carbogen as an intervention);

Basically, the manuscript attached in Appendix a) describes both the methodology and results for this sub-task. Please refer to it for detailed information. Note that although the study reported in the manuscript used primarily prostate tumors, the methodology and the algorithm developed in the study are applicable to breast tumors. The actual ivestigations for breast tumors are underway.

Task 1c: to employ proper algorithms to calculate absolute values and changes of SO_2 and Hb in the tumor vascular bed before, during, and after the respiratory challenge;

The PI and her graduate student, Mengna Xia, have been working on this sub-task, and the status report for this is as follows:

In order to quantify Hb and SO_2 of a measured sample, we have attempted two algorithms.

Algorithm 1 (variation method): According to Matthias Kohl et al.[3,4], small changes in absorption, μ_a, induce changes in both measured reflectance, R, and phase, Φ, and they can be expressed as

$$\begin{aligned} R(\rho) &= z_a(1/\rho + \mu_{eff})\frac{e^{-\mu_{eff}\rho}}{2\pi\rho^2} \\ <t>(\rho) &= \frac{\rho^2}{2c(D+\rho\sqrt{\mu_a D})} \\ \Phi &= -2\pi\nu <t> \end{aligned} \tag{7}$$

where ρ is the source-detector separation, $z_0 = 1/(\mu_a + \mu_s')$, $\mu_{eff}=[3\mu_a(\mu_a+\mu_s')]^{0.5}$, $D=1/(3\mu_s')$, μ_a and μ_s' are absorption and reduced scattering coefficients, respectively, t is time, and ν is the modulation frequency of the diffuse photon density waves traveling in tissues. Based on eq. (7) and defining A as A=log(R), we derived an equation to obtain μ_a:

$$\mu_a = \frac{Q_a}{a} + \frac{1-\sqrt{1+\frac{12\rho^2\mu_s' Q_a}{a}}}{6\rho^2\mu_s'}, \tag{8}$$

where $a=c/[\pi\nu\ln(10)]$ and $Q_a = \Delta A/\Delta\Phi$. Q_a can be obtained by measuring changes in amplitude, ΔA, and phase, $\Delta\Phi$. The condition to employ eq. (8) to quantify μ_a is that the measured sample has to undergo a perturbation so that small changes in both ΔA and $\Delta\Phi$ occur and lead to Q_a determination. Further inspection on Q_a shows that Q_a is largely independent of the scattering property, μ_s', of the medium, as shown in Figure 6 below. This means μ_a obtained from Q_a is largely independent of μ_s' variations.

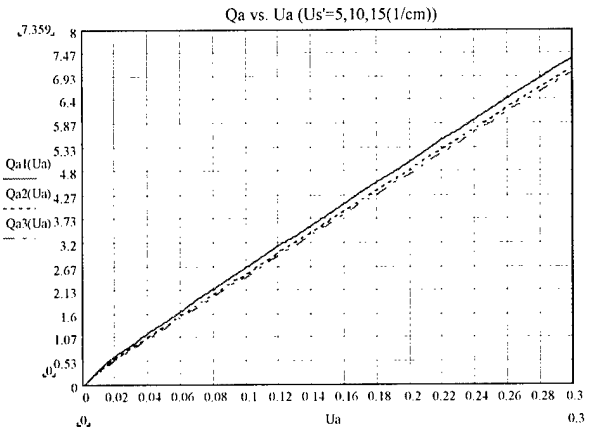

Figure 6. Q_a plot versus μ_a at three different μ_s' values of 5, 10, and 15 cm^{-1}. The differences of Q_a values with different μ_s' are minimal.

Algorithm 2 (Iterative fitting): On the other hand, based on the diffusion approximation with a semi-infinite boundary condition[5], we developed an iterative, curve-fitting program for our single channel (single source-detector separation), two wavelength, IQ system to calculate μ_a and μ_s' values of the measured samples. The prerequisite for this algorithm to be applied is that we have to know one pair of μ_a and μ_s' for calibrating the instrument. In the following is the protocol for the curve-fitting algorithm in getting the μ_a and μ_s' values at different times (or under different conditions):

a) to have a set of known μ_{ao} and μ_{so}' for calibration;
b) to have an initial guess for a set of μ_a and μ_s' to calculate the reflectance, $R(\rho,\omega,\mu_a,\mu_s')$;
c) to compare the calculated $R(\rho,\omega, \mu_a,$ and $\mu_s')$ with the real measured R, and try to decrease the difference between two R's by iteratively changing the values of μ_a and μ_s'. The set of μ_a and μ_s' that give the minimal difference between the two R's is the best fit to the diffusion equation, and thus it is considered to be the μ_a and μ_s' values of the measured sample.

Steps a) to c) can be repeated for different wavelengths, and the determinations of μ_a at two wavelengths result in the calculations of absolute concentrations of [Hb], [HbO_2], and [Hb_{total}], which are derived and expressed as follows:

$$[Hb]=1.1035\ \mu_a^{758} - 0.8583\mu_a^{785} \quad (9)$$

$$[HbO_2]= -1.4331\ \mu_a^{758} + 2.4165\ \mu_a^{785} \quad (10)$$

$$SO_2=[HbO_2]/([HbO_2]+[Hb]) \quad (11)$$

$$[Hb]_{total} = [HbO_2]+[Hb] \quad (12)$$

The following figures, Figures 7-9, show an example of quantifying μ_a, μ_s', and SO_2 from the same blood phantom experiment whose result was shown above in Figure 5:

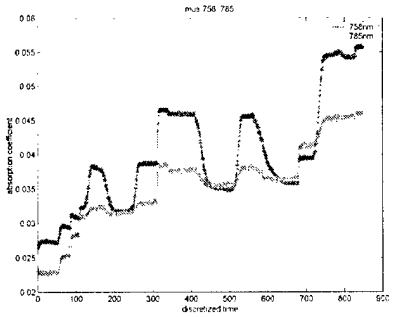

Figure 7. Absorption coefficient plot versus time at two wavelengths, 758nm and 785 nm.

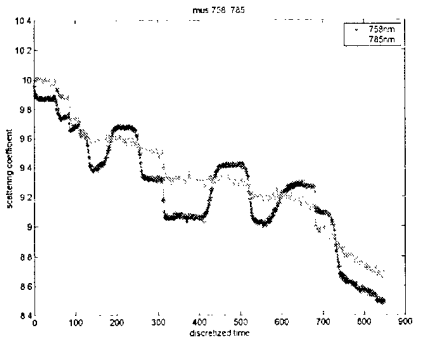

Figure 8. Reduced scattering coefficient plot versus time at two wavelengths, 758nm and 785 nm.

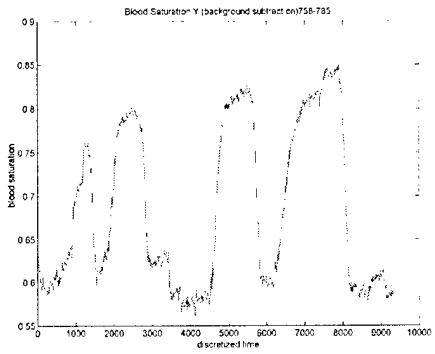

Figure 9. Hemoglobin saturation plot versus time at two wavelengths, 758nm and 785 nm.

For our breast tumor studies, our instrument has only one source-detector separation and two wavelengths, so we have to initially assume a μ_s' value in order to obtain our initial μ_a value, basic on Algorithm 1. Furthermore, we know that μ_s' values of biological tissues are in the range from 5 cm^{-1} to 15 cm^{-1}. For such a range, through computer simulations, we learned that both Algorithm 1 and Algorithm 2 mentioned above are not too sensitive to variations of scattering properties when calculating total hemoglobin concentrations. However, both algorithms have their limitations. For Algorithm 1, it can give only the μ_a value in the period with a perturbation in μ_a, which is induced by changes in hemoglobin concentration. For Algorithm 2, it can give μ_a values only after one set of μ_a and μ_s' is known since we have to use them for calibrating our instrument.

A Combined Algorithm:

Thus, we combined these two algorithms to obtain μ_a of the measured sample during a period of intervention/perturbation. In the following are listed two basic steps:

a) to use Algorithm 1 (i.e., the variation method) to get one μ_a value within a perturbation period, and assume μ_s'=10 cm^{-1};
b) then, to use this determined μ_a, along with μ_s'=10 cm^{-1}, as the calibration value, and apply them in Algorithm 2 (i.e, the iterative fitting) to get μ_a values of the other points in the measured period.

Our studies through computer simulations have shown that the errors caused by the assumption of μ_s'=10 cm^{-1} are within 10-15% if the true μ_s' values of the measured samples are in the range of 5-15 cm^{-1}. Right now, we are conducting laboratory experiments to validate the

combined algorithm for Hb and Hb_{total} calculations and having a manuscript written in 1-2 month to describe the combined algorithm.

Task 1d: to compare the SO_2 values with pO_2 and study vascular and tissue dynamic response to the respiratory change.

Again, the manuscript attached in Appendix a) describes both the methodology and results for this sub-task. Please refer to it for detailed information. Note that although the tumors used in the study were primarily prostate tumors, the methodology and the algorithm developed in the study are applicable to breast tumors. The actual studies for breast tumors are underway.

Key Research Accomplishments

1) We have investigated the relationships between tumor vascular oxygenation and tumor oxygen tensions under carbogen intervention using the NIR spectrometer, pO_2 needle electrodes, and ^{19}F MRI pO_2 mapping. This study demonstrates that the NIRS technology can provide an efficient, real-time, non-invasive approach to monitoring tumor physiology, and emphasizes the need to develop an imaging technique to reveal spatial heterogeneity.

This part of work has been mainly carried by Jae Kim, a Ph.D. graduate student in our BME program.

2) We have developed a combined algorithm that can be used to quantify oxygenated and total hemoglobin concentrations based on our single source-detector separation, two-wavelength, frequency-domain NIR system. This algorithm will be applied to breast tumor measurements for absolute quantifications.
This part of work has been mainly carried by Mengna Xia, a Ph.D. graduate student in our BME program.

3) We have performed a few preliminary studies on
   a. determination of breast tumor oxygen consumption by NIRS ,
   b. vascular oxygen dynamics of breast tumors in response to pharmacological interventions by NIRS,
   c. blood volume quantification in breast tumors by ^{19}F MRS of PFOB and its correlation to $\Delta[Hb]_{Total}$ by NIRS.

This part of work was mainly conducted by Yulin Song, who was a Ph.D. candidate in our Biomedical Engineering Program from 1995 to 2001. He completed his Ph.D. work in August of 2001 with a dissertation title of "Tumor Oxygenation and Physiology in Response to Therapeutic Interventions Investigated by ^{19}F MRI an NIR Spectroscopy." See appendix b for details.

Reportable Outcomes

Manuscripts for Peer-reviewed Journals:

1. Jae G. Kim, Yulin Song, Dawen Zhao, Anca Constantinescu, Ralph P. Mason, and **Hanli Liu**, "Interplay of Tumor Vascular Oxygenation and Tumor pO_2 Observed Using NIRS,

Oxygen Needle Electrode, and ^{19}F MR pO_2 Mapping," submitted to *J. of Biomedical Optics* (2001).

2. Jae Kim and **Hanli Liu**, "Error Analysis of Calculated Hemoglobin Concentrations Caused by Variations of Extinction Coefficients," in preparation and to be submitted to *Optics Express*.
3. Mengna Xia and **Hanli Liu**, "Determination of Total Hemoglobin Concentrations in Blood-Perfused Turbid Meida with Scattering Variations," in preparation and to be submitted to *J. of Biomedical Optics*.

Presentations and Proceeding Papers:

1. **Hanli Liu**, "Near-Infrared Spectroscopy Used in vivo for Assisting Neurosurgery and Tumor Oximetry," Workshop on Biotechnology and Nano-biotechnology—Challenges and Opportunities of Drug Targeting in the Post Genomic Era, organized by the University of Texas at Dallas and the University of Texas Southwestern Medical Center at Dallas, Dallas, October 18, 2001.

2. J. G. Kim, Y. Song, D. Zhao, A. Constantinescu, R. P. Mason, and **Hanli Liu,** "Interplay of Tumor Vascular Oxygenation and pO_2 in Tumors Using NIRS and Needle Electrode," *Proc. SPIE-Int. Soc. Opt. Eng.* 4250, 429-436 (2001).

Degrees obtained that are supported by this award:

Yulin Song was a Ph.D. candidate in our Biomedical Engineering Program from 1995 to 2001. He completed his Ph.D. work in August of 2001 with a dissertation title of "Tumor Oxygenation and Physiology in Response to Therapeutic Interventions Investigated by ^{19}F MRI an NIR Spectroscopy." The current DOD Breast Cancer Grant offered necessary equipment resources and intellectual support for Yulin Song to investigate tumor vascular oxygenation using Near Infrared spectroscopy, while Mr. Song was also funded by the DOD Breast Cancer Research Pre-Doctoral Fellowship from 1997 to 2001 (DAMD17-97-1-7261).

Right now, Dr. Song is a post-doctoral fellow in the Department of Radiology of Stanford University, California.

Conclusions

From the work that we have conducted up-to-date, we can draw the following conclusions:

1) we have measured relative $[HbO_2]$ changes in tumor vasculature and tumor tissue pO_2 under carbogen intervention using NIRS and needle type pO_2 electrode, and the pO_2 data were also supported by the ^{19}F MR pO_2 mapping. The NIRS data showed significant changes in vascular oxygenation accompanying respiratory interventions, and changes in tumor vascular oxygenation preceded tumor tissue pO_2. The correlation between normalized tumor $\Delta[HbO_2]$ and tumor tissue pO_2 shows that there is a threshold of normalized $\Delta[HbO_2]$ for tumor cells to be efficiently oxygenated. This indicates the difficulty of oxygen delivery into the hypoxic regions of tumors.

2) A combined algorithm can be developed for quantifying absolute Hb, HbO_2, and Hb_{total}, and this algorithm is particularly made for our single source-detector separation, two wavelength, NIR system. With this algorithm, we can obtain relatively accurate results in $[Hb_{total}]$ with possible scattering variations.

3) Also, we learned that variations in extinction coefficients can cause significant errors.

References

1. Mark Cope, "The Application of Near Infrared Spectroscopy to Non Invasive Monitoring of Cerebral Oxygenation in the Newborn Infant", Doctoral Thesis of Dept. of Medical Physics and Bioengineering, University College London, England, (1991).

2. W. G. Zijlstra, A. Buursma, H. E. Falke and J. F. Catsburg, "Spectrophotometry of Hemoglobin: Absortion Spectra of Rat Oxyhemoglobin, Deoxyhemoglobin, Carboxyhemoglobin, and Methemoglobin" *Comp. Biochem. Physiol.* **107B**, pp. 161-166, (1994).

3. Matthias Kohl, Russell Watson, Mark Cope. "Optical properties of highly scattering media determined from changes in attenuation, phase and modulation depth" Optical Tomography and Spectroscopy of Tissue: Theory, Instrumentation, Model, and Human Studies II, SPIE Vol. 2979, 365-374 (1997).

4. Matthias Kohl, Russell Watson, Gabriel Chow, Idris Roberts, David Delpy, Mark Cope. "Monitoring of cerebral hemodynamics during open-heart surgery in children using near infrared intensity modulated spectroscopy" Optical Tomography and Spectroscopy of Tissue: Theory, Instrumentation, Model, and Human Studies II, SPIE Vol. 2979, 408-416 (1997).

5. Brian W. Pogue, "Error assessment of a wavelength tunable frequency domain system for noninvasive tissue spectroscopy", *Journal of Biomedical Optics* (2000).

List of Appendixes

a) Manuscript submitted to J. of Biomedical Optics.
b) Table of Contents of Dr. Song's Dissertation.
Among 9 chapters in his dissertation, Chapters 2, 4, 5, 6, 8 described the NIR techniques and methods for breast tumor measurements, showed results and drew conclusions.

[1] Mark Cope, "The Application of Near Infrared Spectroscopy to Non Invasive Monitoring of Cerebral Oxygenation in the Newborn Infant", Doctoral Thesis of Dept. of Medical Physics and Bioengineering, University College London, England, (1991).

[2] W. G. Zijlstra, A. Buursma, H. E. Falke and J. F. Catsburg, "Spectrophotometry of Hemoglobin: Absortion Spectra of Rat Oxyhemoglobin, Deoxyhemoglobin, Carboxyhemoglobin, and Methemoglobin" *Comp. Biochem. Physiol.* **107B**, pp. 161-166, (1994)

[3] Matthias Kohl, Russell Watson, Mark Cope. "Optical properties of highly scattering media determined from changes in attenuation, phase and modulation depth" Optical Tomography and Spectroscopy of Tissue: Theory, Instrumentation, Model, and Human Studies II, SPIE Vol. 2979, 365-374 (1997).

[4] Matthias Kohl, Russell Watson, Gabriel Chow, Idris Roberts, David Delpy, Mark Cope. "Monitoring of cerebral hemodynamics during open-heart surgery in children using near infrared intensity modulated spectroscopy" Optical Tomography and Spectroscopy of Tissue: Theory, Instrumentation, Model, and Human Studies II, SPIE Vol. 2979, 408-416 (1997).

[5] Brian W. Pogue "Error assessment of a wavelength tunable frequency domain system for noninvasive tissue spectroscopy",

Interplay of Tumor Vascular Oxygenation and Tumor pO_2 Observed Using NIRS, Oxygen Needle Electrode, and ^{19}F MR pO_2 Mapping

Jae G. Kim[+], Yulin Song[+ϕ], Dawen Zhao[ϕ], Anca Constantinescu[ϕ],
Ralph P. Mason[ϕ], and Hanli Liu[+]*

[+]Joint Graduate Program in Biomedical Engineering
University of Texas at Arlington/University of Texas Southwestern Medical Center at Dallas
Arlington, TX 76019

[ϕ]Advanced Radiological Sciences, Department of Radiology
University of Texas Southwestern Medical Center at Dallas
Dallas, TX 75390

ABSTRACT

Breathing carbogen (95% O_2, 5% CO_2) to enhance tumor oxygenation may improve tumor response to therapy. However, few studies have been reported on the relationship between tumor oxygen tension (pO_2) and blood oxygenation in tumor vasculature. This study investigates the correlation of tumor blood oxygenation and tumor pO_2 with respect to carbogen inhalation and compares such correlation with that in blood. We used near-infrared spectroscopy (NIRS) to measure changes of oxygenated hemoglobin concentration ($\Delta[HbO_2]$) and used an oxygen needle electrode and ^{19}F MRI for pO_2 measurements in tumors. The measurements were taken from Dunning prostate R3327 tumors implanted in rats, while the rats were anesthetized breathing air or carbogen. In the tissue-phantom study, 1% intralipid solution and rabbit blood were used. NIRS results showed significant changes in tumor vascular oxygenation in response to carbogen inhalation. Furthermore, the results show an apparent threshold for tumor pO_2 response. The slope of pO_2 versus normalized $\Delta[HbO_2]$ below the threshold obtained from the tissue phantom was ten times larger than the slope from the tumor, indicating that tumor cells are much harder to oxygenate. This study demonstrates that the NIRS technology can provide an efficient, real-time, non-invasive approach to monitoring tumor physiology and is complementary to other techniques.

Key Words: Frequency-Domain Spectroscopy, NIR Spectroscopy, ^{19}F MRI, Tumor Vascular Oxygenation, pO_2 electrode, Oxygen, Oximetry

* hanli@uta.edu; phone 1 817 272-2054; fax 1 817 272-2251; Joint Program of Biomedical Engineering, P.O. Box 19138, University of Texas at Arlington, Arlington, TX, USA 76019-0167

1. Introduction

It has long been known that hypoxic tumor cells are more resistant to radiation therapy than well-oxygenated tumor cells.[1] Breathing elevated oxygen (100%) or carbogen (95% O_2, 5% CO_2) has been used during therapy to improve oxygenation.[2,3] However, little is known about oxygen transfer from the tumor vasculature to tumor tissue cells. In this study, we investigated the relationship between vascular oxygenation and tissue oxygenation during respiratory challenge in rat prostate tumors using Near-Infrared Spectroscopy (NIRS), pO_2 needle electrodes, and ^{19}F MRI for simultaneous or sequential measurements.

While various methods are available for measuring tissue oxygen tension[4], many of them are highly invasive precluding the detection of dynamic changes. Oxygen microelectrodes[5], fiber optic sensors[6], and electron spin resonance[7] do facilitate measurement of dynamic changes. MRI has the further advantage of providing dynamic maps of pO_2, which can reveal tumor heterogeneity.[8] While NIRS does not quantify pO_2, it can indicate dynamic changes in vascular oxygenation and has the advantage of being entirely non-invasive, providing real-time measurements, and being cost effective and portable.

Oxygenated and deoxygenated hemoglobin molecules are major chromophores in tissue in the near infrared region (700-900 nm), and they exhibit distinct absorption characteristics. In principle, by measuring light absorption and scattering in tissue, the concentrations of oxygenated hemoglobin, [HbO_2], deoxygenated hemoglobin, [Hb], and oxygen saturation of hemoglobin, SO_2, can be determined based on diffusion theory. However, the theory works well only for large and homogeneous media.[9,10] Accurate quantification of tumor

oxygenation in our approach is currently limited to relative changes in $[HbO_2]$ and $[Hb]_{total}$ due to considerable heterogeneity and finite size of tumors.

The goal of this study was to investigate the correlation of tumor blood oxygenation and tumor pO_2 in response to carbogen intervention and to compare such correlation with that from regular tissues using phantoms.

2. Materials and Methods

2.1 Tumor Model and pO_2 needle electrode measurements

Dunning prostate rat tumors (three R3327-HI and two R3327-AT1)[11] were implanted in pedicles on the foreback of adult male Copenhagen rats, as described in detail previously.[12] Once the tumors reached approximately 2 cm in diameter, the rats were anesthetized with 0.2 ml ketamine hydrochloride (100 mg/mL; Aveco, Fort Dodge, IA) and maintained under general gaseous anesthesia with isoflurane in air (1.3% isoflurane at 1 dm^3/min air) through a mask placed over the mouth and nose. Tumors were shaved to improve optical contact for transmitting light. Body temperature was maintained by a warm water blanket and was monitored by a rectally inserted thermal probe connected to a digital thermometer (Digi-Sense, model 91100-50, Cole-Parmer Instrument Company, Vernon Hills, IL). A pulse oximeter (model 8600, Nonin, Inc., Plymouth, MN) was placed on the hind foot to monitor arterial oxygenation (S_aO_2).

Figure 1 shows the schematic setup for animal experiments using NIRS and a pO_2 needle electrode. A needle type oxygen electrode was placed in the tumor, and the reference electrode was placed rectally. The

electrodes were connected to a picoammeter (Chemical Microsensor, Diamond Electro-Tech Inc., Ann Arbor, MI) and polarized at - 0.75 V. Linear two-point calibrations were performed with air (21% O_2) and pure nitrogen (0% O_2) saturated saline buffer solutions before the electrode was inserted into the tumor and we estimated an instrumental precision of 1 mmHg. PO_2 experimental data were manually recorded, while the NIRS data were acquired automatically. Measurements of pO_2 and NIRS were initiated while rats breathed air for ~10 minutes to demonstrate a stable baseline. The inhaled gas was then switched to carbogen for 15 minutes and switched back to air.

2.2 NIR Spectroscopy

NIR spectroscopy can be used to measure hemoglobin concentrations and oxygen saturation because light absorptions of HbO_2 and Hb are different at the wavelengths selected (758 nm and 785 nm). In common with our previous work[13], we assumed that HbO_2 and Hb are the only significant absorbing materials in tumors within the NIR range. The absorption coefficients comprise the extinction coefficients for deoxyhemoglobin (ε_{Hb}) and oxyhemoglobin (ε_{HbO2}) multiplied by their respective concentrations (Equations 1 and 2).

$$\mu_a^{758} = \varepsilon_{Hb}^{758}[Hb] + \varepsilon_{HbO2}^{758}[HbO_2], \quad (1)$$

$$\mu_a^{785} = \varepsilon_{Hb}^{785}[Hb] + \varepsilon_{HbO2}^{785}[HbO_2]\,. \quad (2)$$

An NIR homodyne frequency-domain photon migration system allows one to obtain absorption and scattering properties of the measured sample[14]. Figure 1 indicates the working principle of the NIR system, and detailed

information on the instrument is given elsewhere[13]. We have not yet completed a suitable algorithm to compute μ_a and μ_s' of rat tumors due to their finite size and high heterogeneity. The data presented here were analyzed using only amplitude values to find changes in $[HbO_2]$ and $[Hb]_{total}$, based on modified Beer-Lambert's law (Equation 3). By manipulating Equations 1-3, changes of $[HbO_2]$ and $[Hb]_{total}$ due to respiratory intervention were calculated from the transmitted amplitude of the light through the tumor (Equations 4 and 5).

$$\Delta\mu_a = \mu_{aT} - \mu_{aB} = LN(A_B/A_T) / L, \quad (3)$$

$$\Delta[HbO_2] = [-5.73*LN(A_B/A_T)^{758} + 9.67*LN(A_B/A_T)^{785}] / L, \quad (4)$$

$$\Delta[Hb]_{total} = \Delta[Hb] + \Delta[HbO_2] = [-1.32*LN(A_B/A_T)^{758} + 6.23*LN(A_B/A_T)^{785}] / L, \quad (5)$$

where A_B = baseline amplitude; A_T = transient amplitude; L = optical pathlength between source/detector; the constants given in the equations were computed with the extinction coefficients for oxy- and deoxy-hemoglobin at the two wavelengths used.[15] In principle, the units of $\Delta[HbO_2]$ and $\Delta[Hb]_{total}$ are mM, and L is equal to the source–detector separation multiplied by a Differential Pathlength Factor (DPF)[16]. The DPF has been studied intensively for muscles[17]and brains[18] with approximate values of 4-6 and 5-6, respectively. Little is known about the DPF for tumors, though a DPF value of 2.5 has been used by others[19]. Since our focus is on dynamic changes and relative values of tumor $[HbO_2]$ with respect to carbogen intervention, we have taken the approach of including the DPF in the unit, viz. modifying eq. (4) as follows:

$$\Delta[HbO_2] = [-5.73*LN(A_B/A_T)^{758} + 9.67*LN(A_B/A_T)^{785}] / d, \quad (6)$$

where d is the direct source-detector separation in cm, and the unit of $\Delta[HbO_2]$ in eq. (6) is mM/DPF. We further

will show that our conclusion on the relationship between tumor $\Delta[HbO_2]$ and pO_2 will not be affected by the DPF after normalizing the experimental $\Delta[HbO_2]$ data to its maximal value.

2.3 MRI Instrumentation and Procedure

To support the findings obtained from the pO_2 electrode measurements and NIRS, we conducted MRI experiments using an Omega CSI 4.7 T 40 cm system with actively shielded gradients. A homebuilt tunable $^1H/^{19}F$ single turn solenoid coil was placed around the tumor. 45 μL of hexafluorobenzene (HFB; Lancaster, Gainesville, FL) was administered directly into the tumor using a Hamilton syringe (Reno, NV) with a custom-made fine sharp (32 gauge) needle with deliberate dispersion along several tracks to interrogate both central and peripheral tumor regions as described in detail previous[6]. HFB is ideal for imaging pO_2, because it has a single resonance, and its relaxation rate varies linearly with oxygen concentration. ^1H images were acquired for anatomical reference using a traditional 3D spin-echo pulse sequence. Conventional ^{19}F MR images were then taken to show the 3D distribution of the HFB in the tumor. ^{19}F MR images were directly overlaid over ^1H images to show the position of the HFB in that slice.

Tumor oxygenation was assessed using FREDOM (Fluorocarbon Relaxometry using Echo planar imaging for Dynamic Oxygen Mapping) based on ^{19}F pulse burst saturation recovery (PBSR) echo planar imaging (EPI) of HFB. The PBSR preparation pulse sequence consists of a series of 20 non-spatially selective saturating 90° pulses with 20 ms spacing to saturate the ^{19}F nuclei. Following a variable delay time τ, a single spin-echo EPI

sequence with blipped phase encoding was applied.[20] Fourteen 32×32 PBSR-EPI images, with τ ranging from 200 ms to 90 sec and a field of view (FOV) of 40×40 mm, were acquired in eight minutes using the ARDVARC (Alternated Relaxation Delays with Variable Acquisitions to Reduce Clearance effects) acquisition protocol[21]. An $R1$(=1/T1) map was obtained by fitting signal intensity of each voxel of the fourteen images to a three parameter relaxation model by Levenberg-Marquardt least squares algorithm (equation 6):

$$y_n(i,j) = A(i,j) \cdot [1 - (1+W) \cdot \exp(-R1(i,j) \cdot \tau_n)] \quad (6)$$
$$(n = 1, 2, \cdots\cdots, 14)$$
$$(i, j = 1, 2, \cdots\cdots, 32)$$

where $y_n(i,j)$ is the measured signal intensity corresponding to delay time τ_n (the nth images) for voxel (i,j), $A(i,j)$ is the fully relaxed signal intensity amplitude of voxel (i,j), W is a dimensionless scaling factor allowing for imperfect signal conversion, and $R1(i,j)$ is the relaxation rate of voxel (i,j) in unit of sec^{-1}. A, W and $R1$ are the three fit parameters for each of the 32 x 32 voxels. Finally, the pO_2 maps were generated by applying the calibration curve: $pO_2(mmHg) = [R1(s^{-1}) - 0.0835]/0.001876$ at 37 °C to the $R1$ maps.[21]

2.4 Tissue Phantom Solution Model

The tissue-simulating phantom comprised a solution of 1% Intralipid in saline buffer. The oxygen needle electrode, a pH electrode and a thermocouple probe (model 2001, Sentron, Inc., Gig Harbor, WA) were placed in the solution, and a gas tube was placed opposite the NIRS probes to minimize any liquid movement effects (Figure 2). Source and detector probes for the NIRS were placed in reflection geometry. The solution was stirred

at ~ 37 °C to maintain homogeneity. Fresh whole rabbit blood (2 ml) was added to the 200 mL solution before baseline measurement. Nitrogen gas and air were used to deoxygenate and oxygenate the solution, respectively.

3. Results

3.1 Tumor Study Results

Figure 3a shows the temporal profiles of $\Delta[HbO_2]$ and pO_2 in a small Dunning prostate R3327-HI tumor (1.5 cm^2) with respiratory challenge measured simultaneously with NIRS and the pO_2 needle electrode. After a switch from air to carbogen, $\Delta[HbO_2]$ increased rapidly, along with tumor tissue pO_2. Figure 3b was obtained from a second large prostate tumor (3.1 cm^2) and now the NIRS response was biphasic, while the electrode showed a slower pO_2 response. In a third tumor NIRS behaved as before, but pO_2 did not change (Fig. 3c).

In two tumors from a separate subline (Dunning prostate R3327-AT1), NIRS and ^{19}F MRI were taken with carbogen challenge sequentially (Fig. 4). NIRS response showed vascular oxygenation changes as before, and FREDOM revealed the distinct heterogeneity of the tumor tissue response. Initial pO_2 was in the range of 1 to 75 mmHg and carbogen challenge produced values in the range 6 to 360 mmHg. Representative voxels are shown.

3.2 Tissue Phantom Solution Study Results

Figure 5 shows a similar temporal profile for $\Delta[HbO_2]$ and pO_2 measured from the tissue phantom during a cycle of gas change from air to nitrogen and back. The first five minutes were measured as a baseline after adding 2 ml blood. Bubbling nitrogen deoxygenated the solution and caused the pO_2 values to fall; $\Delta[HbO_2]$

declined accordingly with a small time lag. After the bubbling gas was switched from nitrogen to air, both $\Delta[HbO_2]$ and pO_2 started to increase simultaneously, but the recovery time of $\Delta[HbO_2]$ to the baseline was faster than that of pO_2. The small time lag between the changes of $\Delta[HbO_2]$ and pO_2 is probably due to the allosteric interactions between hemoglobin and oxygen molecules. According to the hemoglobin oxygen-dissociation curve[22, 23], oxyhemoglobin starts to lose oxygen significantly when pO_2 falls below 70 mmHg at standard conditions (pH=7.4 and temperature=37 °C). The same principle can explain why $\Delta[HbO_2]$ has a faster recovery than that of pO_2. Namely, $\Delta[HbO_2]$ became saturated as pO_2 increased from 0 to 70 mmHg, while the solution was being oxygenated. Importantly, $\Delta[Hb]_{total}$ remained unchanged, as expected, during the cycle of deoxygenation and oxygenation.

3.3 Correlation of pO_2 and $\Delta[HbO_2]/\Delta[HbO_2]_{max}$

To compare the data from tumors and the phantom for the relationship between changes in tumor vascular oxygenation and tumor tissue pO_2, we normalized $\Delta[HbO_2]$ at the maximum value during the carbogen intervention, i.e., $\Delta[HbO_2]/\Delta[HbO_2]_{max}$. One advantage of using normalized $\Delta[HbO_2]$ is to eliminate the uncertainty of DPF.

Figure 6a replots the data given in figures 3a and 3b, showing a direct relationship between the normalized $\Delta[HbO_2]$ and pO_2 in the tumors measured with NIRS and the pO_2 needle electrode. It shows that pO_2 in the tumors varied linearly with a slope of 4.1 in case 1 and a slope of 3.6 in case 2 before $\Delta[HbO_2]$ reached 80 % and

60 % of $\Delta[HbO_2]_{max}$ in cases 1 and 2, respectively. Thereafter, tumor pO_2 increased sharply, indicating a threshold for tumor tissue pO_2 to increase. While NIRS results tended to be similar for several tumors, pO_2 electrode measurements showed considerable variation even in the same tumor type, suggesting distinct tumor heterogeneity. This was substantiated by the ^{19}F MR pO_2 mappings: indeed, in some cases, pO_2 values did not change with respiratory challenge, especially when baseline pO_2 values were lower than 10 mmHg.

Figure 6b shows the relationship between normalized $\Delta[HbO_2]$ and pO_2 measured from the phantom. The threshold occurred at essentially the same value of $\Delta[HbO_2]/\Delta[HbO_2]_{max}$ (~80%) as observed for tumor case 2. However, the phantom showed a much larger slope between pO_2 and $\Delta[HbO_2]/\Delta[HbO_2]_{max}$, i.e., 39.5, prior to the threshold.

Figure 6c summarizes the data obtained from the tumors and phantom and plots them with reversed axes. In the phantom, pO_2 had increased from 0 mmHg to 70 mmHg by the stage that $\Delta[HbO_2]$ reached to 90% of $\Delta[HbO_2]_{max}$. This behavior is reminiscent of the hemoglobin oxygen dissociation curve. By comparison, the tumor pO_2 increased only from 14 mmHg to 30 mmHg in case 1 and from 10 mmHg to 21 mmHg in case 2 when $\Delta[HbO_2]$ approached to 90 % of $\Delta[HbO_2]_{max}$.

4. Discussion and conclusion

Tumor oxygenation involves a complex interplay of multiple compartments and parameters: blood flow, blood volume, blood vessel structure, and oxygen consumption. NIRS provides a global non-invasive estimate of

average vascular oxygenation encompassing arterial, venous and capillary compartments. In agreement with our previous observations[13], the $\Delta[HbO_2]$ response is often biphasic, which we believe represents rapid elevation of arterial oxygenation, followed by more sluggish capillary components. Comparison with electrode measurements indeed revealed that tumors are heterogeneous. Like an NIRS measurements, pO_2 electrodes provide rapid assessment of pO_2 facilitating real time observation of dynamic changes. In Fig. 3a, pO_2 starts at a baseline value ~ 15 mmHg and increases rapidly in response to respiratory challenge with carbogen. Indeed, the rate approaches that of the vascular compartments. In a second tumor, where the interrogated location showed a slightly lower pO_2, the tissue response was more sluggish (Fig. 3b). For a third HI tumor, local baseline pO_2 was found to be < 5 mmHg and this did not changed with carbogen inhalation despite the response observed by NIRS. This suggests a danger of comparing a global vascular measurement with regional tumor pO_2, since tumors are known to be highly heterogeneous.

Indeed, FREDOM measurements in Fig. 4 revealed the heterogeneity in baseline oxygenation within individual tumors of this second tumor subline. Baseline pO_2 ranged from 1 – 75 mmHg and response to carbogen was variable in terms of rate and extent, as seen for the HI subline using electrodes. As with the electrodes, the better oxygenated tumor regions showed a faster and greater response to carbogen inhalation.

The phantom measurements indicate the reliability of the NIRS technique. Both phantom and tumor measurements indicate a sharp increase of pO_2 after the normalized $\Delta[HbO_2]$ reaches about 80% of its maximum. This coincides with the recognized sigmoidal binding of oxygen to hemoglobin. The difference between the

phantom and tumor results reveals that the pO_2 response to $[HbO_2]$ changes in tumor is about 10 times smaller than that in tissue phantom when pO_2 values are relatively low (0 to 30 mmHg). This demonstrates a greater hurdle to delivering oxygen from blood vasculature into the hypoxic regions of the tumor than into regular tissues. The slope at low $\Delta[HbO_2]/\Delta[HbO_2]_{max}$ in the tumors presumably also reflects oxygen consumption by the tumor tissues, as oxygen initially becomes available.

Both NIRS and electrodes offer essentially real time measurement of changes in oxygenation, which can be rapid (Fig. 3). Indeed, the inflow kinetics of vascular O_2 detected by NIRS are similar to those previously reported in the HI tumor line following a bolus of the paramagnetic contrast agents Gd-DTPA[24]. FREDOM has lower temporal resolution, but reveals the tumor heterogeneity and differential response of regions exhibiting diverse baseline pO_2. The results here correspond closely with more extensive observation[6, 8, 21]. While FREDOM currently requires 6½ minutes per pO_2 map, we have previously demonstrated alternative data acquisition protocol achieving 1 s time resolution in a perfused heart, albeit providing less precision in measurements and only a global determination.[25]

In conclusion, we have measured relative $[HbO_2]$ changes in tumor vasculature and tumor tissue pO_2 under carbogen intervention using NIRS and needle type pO_2 electrode, and the pO_2 data were also supported by the ^{19}F MR pO_2 mapping. The NIRS data showed significant changes in vascular oxygenation accompanying respiratory interventions, and changes in tumor vascular hemoglobin oxygenation preceded tumor tissue pO_2. The correlation between normalized tumor $\Delta[HbO_2]$ and tumor tissue pO_2 shows that there is a threshold of normalized $\Delta[HbO_2]$

for tumor cells to be efficiently oxygenated. This indicates the difficulty of oxygen delivery into the hypoxic regions of tumors. This study demonstrates that the NIRS technology can provide an efficient, real-time, non-invasive approach to monitoring tumor physiology, and emphasizes the need to develop an imaging technique to reveal spatial heterogeneity.

Acknowledgement

This work was supported in part by The Whitaker Foundation (HL), NIH RO1 CA79515 (RPM), and the Department of Defense Breast Cancer Initiative grant BC990287 (HL). NMR experiments were conducted at the Mary Nell & and Ralph B. Rogers MR center, an NIH BRTP Facility no. 5-P41-RR02584. We are grateful to Sherwin Yen and William McSweeny for assistance with data acquisition and Dr. Peter Peschke for providing the original tumor cells.

Figure Captions

Figure 1. Schematic experimental setup of one channel, near infrared, frequency domain IQ instrument for tumor investigation *in vivo*. The 5-mm diameter fiber bundles deliver the laser light, comprising two wavelengths (758 and 785 nm) and detect the laser light following absorption through the implanted tumor. The pO_2 needle electrode measures tumor tissue pO_2.

Figure 2. Experimental setup for phantom study using 1% Intralipid in saline buffer. NIRS probes were placed in reflectance mode, while the gas bubbler was placed opposite to minimize liquid movement effects. After adding 2 ml of rabbit blood to a 200 ml solution, nitrogen gas and air were introduced to deoxygenate and oxygenate the solution, respectively.

Figure 3. Simultaneous dynamic changes of $\Delta[HbO_2]$ and pO_2 in R3327-HI rat prostate tumors using NIRS and pO_2 needle electrode; (a) A smaller tumor (1.5 cm^3) showed a rapid pO_2 response (Case 1), whereas (b) a bigger tumor (3.1 cm^3) showed a slower pO_2 response (Case 2). (c) In a third tumor where regional baseline pO_2 was < 5 mmHg, there was no pO_2 response (Case 3). The unit of $\Delta[HbO_2]$ is mM/DPF, where DPF is equal to the optical path length divided by the source-detector separation. Dotted vertical line marks the time when the gas was changed. The oxygen needle electrode was placed in tumors where pO_2 had a baseline value of about 10 mmHg.

Figure 4. Dynamic changes of $\Delta[HbO_2]$ and pO_2 in R3327-AT1 rat prostate tumors measured using NIRS and ^{19}F MR pO_2 mapping. The solid curve represents $\Delta[HbO_2]$ and the solid line with solid circles represents mean $pO_2 \pm$ SE (Standard Error) of 21 (Fig. 4a) and 45 (Fig. 4b) voxels of each tumor. Dashed lines are 4 representative voxels for each case. After a gas switches from air to carbogen, both the mean pO_2 of each tumor increased. Individual voxels showed totally different response, indicating heterogeneity. The tumor sizes were 3.2 cm^3 and 2.7 cm^3 for (a) and (b), respectively.

Figure 5. Simultaneous dynamic changes of $\Delta[HbO_2]$, $\Delta[Hb]_{total}$ and pO_2 in the solution phantom measured using NIRS and pO_2 needle electrode. The dark solid curve is for $\Delta[HbO_2]$, the lighter solid line is for $\Delta[Hb]_{total}$, and the solid circles show pO_2 values in the phantom solution. After ~3 minutes of baseline, the bubbling gas was changed from air to nitrogen to deoxygenate the solution and then switched back to air to reoxygenate the solution. The unit of $\Delta[HbO_2]$ is mM/DPF.

Figure 6. Changes of tumor tissue pO_2 with normalized changes of oxygenated hemoglobin (a) in tumors measured with NIRS and a pO_2 needle electrode, and (b) in the phantom solution using the same NIRS and pO_2 needle electrode. The slope between pO_2 and $\Delta[HbO_2]/\Delta[HbO_2]_{max}$ is 3.6 when $\Delta[HbO_2]/\Delta[HbO_2]_{max}$ is less than 0.8 in Case 2 tumor, while the slope obtained from the phantom solution is 39.5, which is ten times larger than that in Case 2. (c) Summarizing of relationship between pO_2 and normalized $\Delta[HbO_2]$ obtained from both tumors

and the tissue phantom. Dotted horizontal line shows 90% of normalized $\Delta[HbO_2]$.

References:

1. L. Gray, A. Conger, M. Ebert, S. Hornsey and O. Scott, "The concentration of oxygen dissolved in tissues at time of irradiation as a factor in radio-therapy," *Br. J. Radiol.*, **26**, pp. 638-648 (1953)

2. J. H. Kaanders, L. A. Pop, H. A. Marres, J. Liefers, F. J. van den Hoogen, W. A. van Daal, A. J. and van der Kogel, "Accelerated radiotherapy with carbogen and nicotinamide (ARCON) for laryngeal cancer," *Radiother. Oncol.*, **48**, pp. 115-22. (1998)

3. J. Overgaard and M. R. Horsman, "Modification of hypoxia-induced radioresistance in tumors by the use of oxygen and sensitizers," *Semin. Radiat. Oncol.*, **6**, pp. 10-21. (1996)

4. H. B. Stone, J. M. Brown and T. Phillips, "Oxygen in human tumors: correlations between methods of measurement and response to therapy," *Radiat. Res.*, **136**, pp. 422-434 (1993)

5. D. Cater and I. Silver, "Quantitative measurements of oxygen tension in normal tissues and in the tumors of patients before and after radiotherapy," *Acta Radiol.*, **53**, pp. 233-256 (1960)

6. D. Zhao, A. Constantinescu, E. W. Hahn and R. P. Mason. "Tumor oxygenation dynamics with respect to growth and respiratory challenge: Investigation of the Dunning prostate R3327-HI tumor," *Radiat. Res.*, **156(5)**, pp. 510-520 (2002)

7. J. A. O' Hara, F. Goda, E. Demidenko and H. M. Swartz, "Effect on regrowth delay in a murine tumor of scheduling split-dose irradiation based on direct pO_2 measurements by electron paramagnetic resonance

Oximetry," *Radiat. Res.*, **150**, pp. 549-56 (1998)

8. R. P. Mason, A. Constantinescu, S. Hunjan, D. Le, E. W. Hahn, P. P. Antich, C. Blum and P. Peschke, "Regional tumor oxygenation and measurement of dynamic changes," *Radiat. Res.*, **152**, pp. 239-249 (1999)

9. M. S. Patterson, B. Chance and B. C. Wilson, "Time resolved reflectance and transmittance for the non-invasive measurement of tissue optical properties," *Appl. Opt.*, **28**, pp. 2331-2336 (1986)

10. E. M. Sevick, B. Chance, J. Leigh, S. Nokia and M. Maris, "Quantitation of time- and frequency-resolved optical spectra for the determination of tissue oxygenation," *Anal. Biochem.*, **195**, pp. 330-351 (1991)

11. P. Peschke, E. W. Hahn, F. Lohr, F. Brauschweig, G. Wolber, I. Zuna and M. Wannenmacher, "Differential sensitivity of three sublines of the rat Dunning prostate tumor system R3327 to radiation and/or local tumor hyperthermia," *Radiat. Res.*, **150**, pp. 423-430 (1998)

12. E. W. Hahn, P. Peschke, R. P. Mason, E. E. Babcock and P. P. Antich, "Isolated tumor growth in a surgically formed skin pedicle in the rat: a new tumor model for NMR studies," *Magn. Reson. Imaging*, **11**, pp. 1007-1017 (1993)

13. H. Liu, Y. Song, K. L. Worden, X. Jiang, A. Constantinescu and R. P. Mason, "Noninvasive investigation of blood oxygenation dynamics of tumors by near-infrared spectroscopy," *Appl. Opt.*, **39**, pp. 5231-5243 (2000)

14. Y. Yang, H. Liu, X. Li and B. Chance, "Low-cost frequency-domain photon migration instrument for tissue spectroscopy, oximetry, and imaging," *Opt. Eng.*, **36**, pp. 1562-1569 (1997)

15. S. J. Matcher, C. E. Elwell, C. E. Cooper, M. Cope and D. T. Delpy, "Performance Comparison of Several Published Tissue Near-Infrared Spectroscopy Algorithms", *Anal. Biochem.*, **227**, pp. 54-68 (1995)

16. J. S. Ultman and C. A. Piantadosi, "Differential pathlength factor for diffuse photon scattering through tissue by a pulse-response method", *Math. Biosci.*, **107(1)**, pp. 73-82 (1991)

17. M. Ferrari, Q. Wei, L. Carraresi, R. A. De Blasi and G. Zaccanti, "Time-resolved spectroscopy of human forearm", *J. Photochem. Photobiol.*, **16**, pp. 141-153, (1992)

18. P. van der Zee, M. Cope, S. R. Arridge, M. Essenpreis, L. A. Potter, A. D. Edwards, J. S. Wyatt, D. C. McCormick, S. C. Roth, E. O. R. Reynolds and D. T. Delpy, "Experimentally measured optical pathlengths for the adult head, calf and forearm and the head of the newborn infants as a function of inter optode spacing", *Adv. Exp. Med. Biol.*, **316**, pp. 143-153, (1992)

19. R. G Steen, K. Kitagishi and K. Morgan, " *In vivo* measurement of tumor blood oxygenation by near-infrared spectroscopy: Immediate effects of pentobarbital overdose or carmustine treatment", *J. Neuro-Oncol.*, **22**, pp. 209-220 (1994)

20. B. R. Barker, R. P. Mason, N. Bansal and R. M. Peshock, "Oxygen tension mapping by ^{19}F echo planar NMR imaging of sequestered perfluorocarbon," *JMRI,* **4**, pp. 595-602 (1994)

21. S. Hunjan, D. Zhao, A. Constantinescu, E. W. Hahn, P. Antich and R. P. Mason, "Tumor oximetry: demonstration of an enhanced dynamic mapping procedure using fluorine-19 echo planar magnetic resonance

imaging in the dunning prostate R3327-AT1 rat tumor," *Int. J. Radiat. Oncol. Biol. Phys.*, **49**, pp. 1097-1108 (2001)

22. R. L. Fournier, "Oxygen transport in biological systems," Chap. 4 in Basic Transport Phenomena in Biomedical Engineering, pp. 87-94, Taylor & Francis, Lillington (1999)

23. S. I. Fox, "Respiratory physiology," Chap. 16 in Human Physiology, pp. 508-513, The McGraw-Hill companies, Inc., Boston (1999)

24. G. Brix, J. Debus, M. Mueller-Schimpfle, P. Peschke, P. Huber, H. J. Zabel and W. Lorenz, "MR-tomographische Quantifizierung struktureller und funktioneller Gewebeveraenderungen an stosswellen-therapierten Dunning-Prostata-Tumoren," *Z. Med. Phys.*, **3**, pp. 76-82 (1993)

25. R. P. Mason, F. M. H. Jeffrey, C. R. Malloy, E. E. Babcock and P. P. Antich, "A noninvasive assessment of myocardial oxygen tension: ^{19}F NMR sepectroscopy of sequestered perfluorocarbon emulsion," *Magn. Reson. Med.*, **27**, pp. 310-317 (1992)

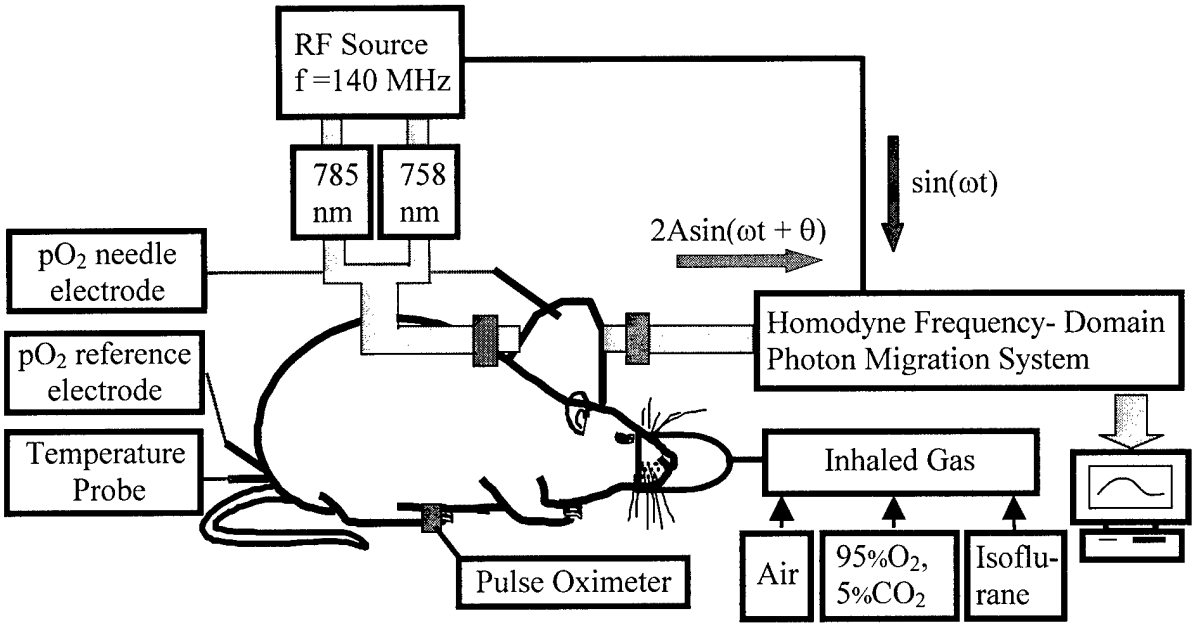
RF Source
f =140 MHz
785 nm
758 nm
sin(ωt)
2Asin(ωt + θ)
pO2 needle electrode
pO2 reference electrode
Temperature Probe
Homodyne Frequency- Domain Photon Migration System
Inhaled Gas
Pulse Oximeter
Air
95%O2, 5%CO2
Isoflu-rane

Figure 1

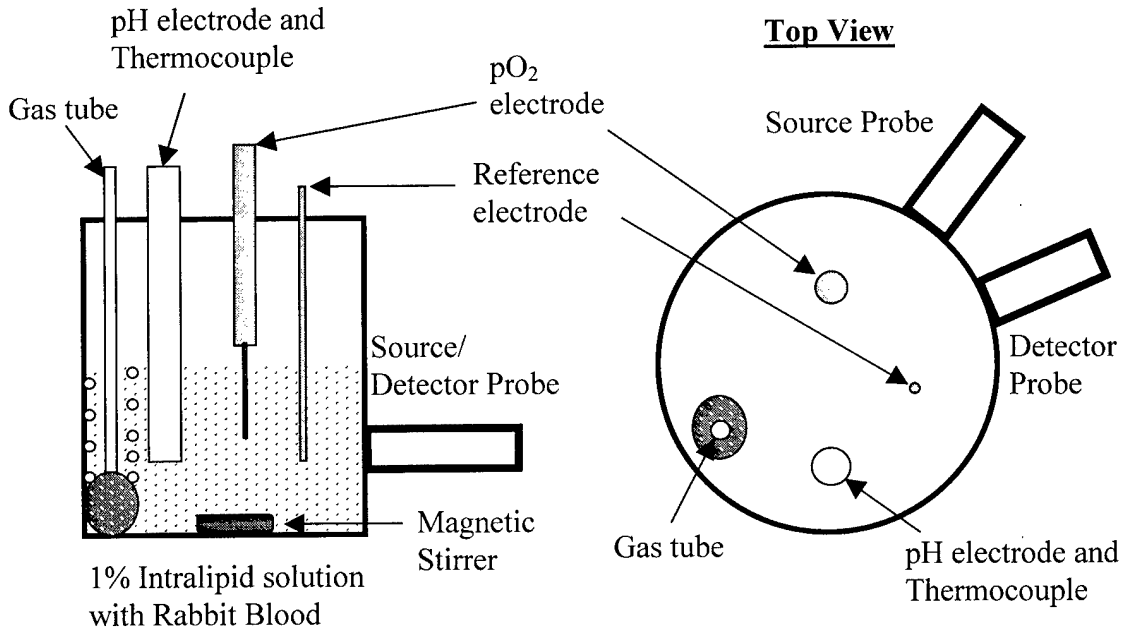
pH electrode and
Thermocouple
Gas tube
pO_2
electrode
Reference
electrode
Source/
Detector Probe
Magnetic
Stirrer
1% Intralipid solution
with Rabbit Blood
Top View
Source Probe
Detector
Probe
Gas tube
pH electrode and
Thermocouple

Figure 2

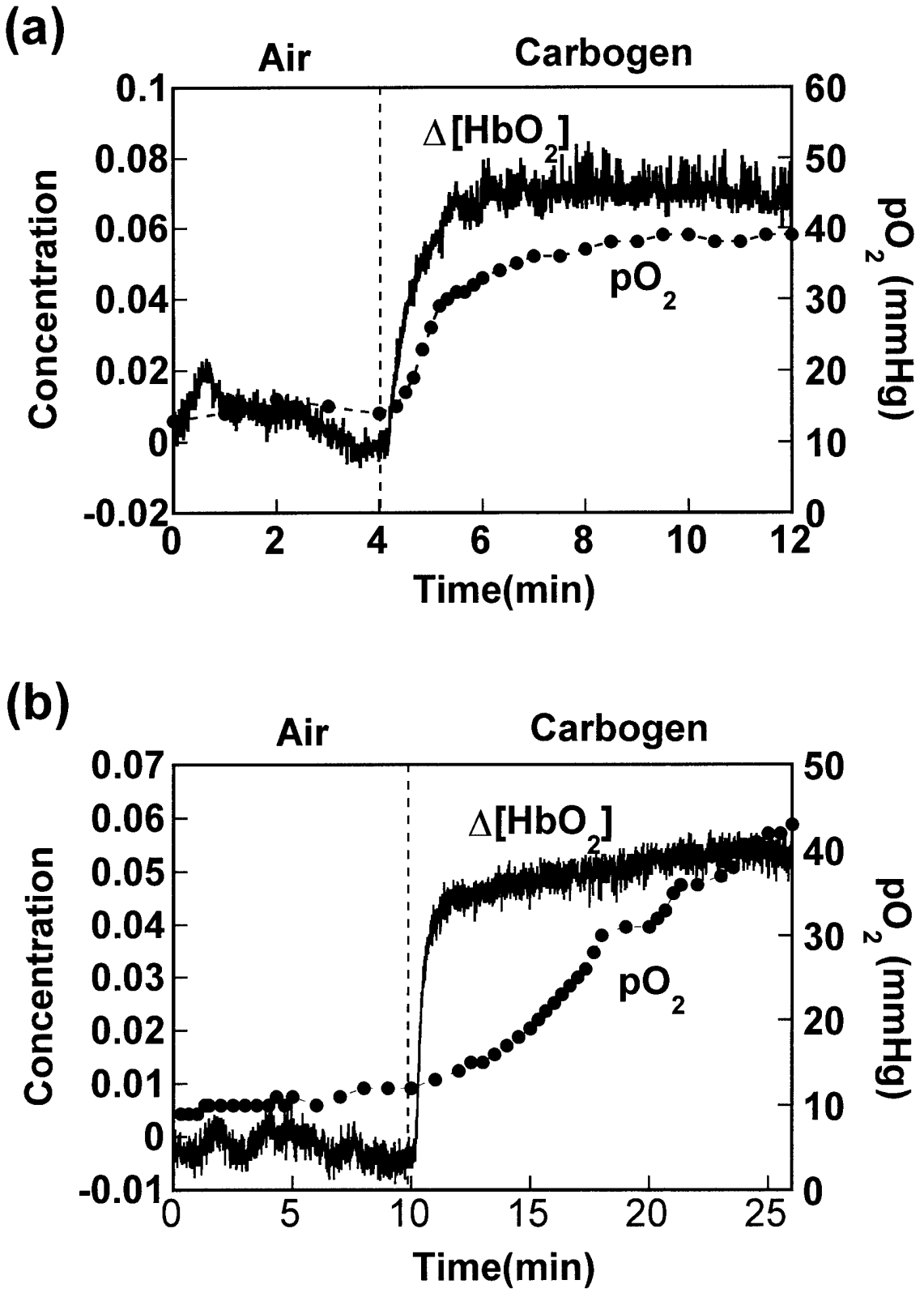
(a)
Air
Carbogen
0.1
0.08
0.06
0.04
0.02
0
-0.02
Concentration
Δ[HbO2]
pO2
60
50
40
30
20
10
0
pO2 (mmHg)
0
2
4
6
8
10
12
Time(min)
(b)
Air
Carbogen
0.07
0.06
0.05
0.04
0.03
0.02
0.01
0
-0.01
Concentration
Δ[HbO2]
pO2
50
40
30
20
10
0
pO2 (mmHg)
0
5
10
15
20
25
Time(min)

Figure 3

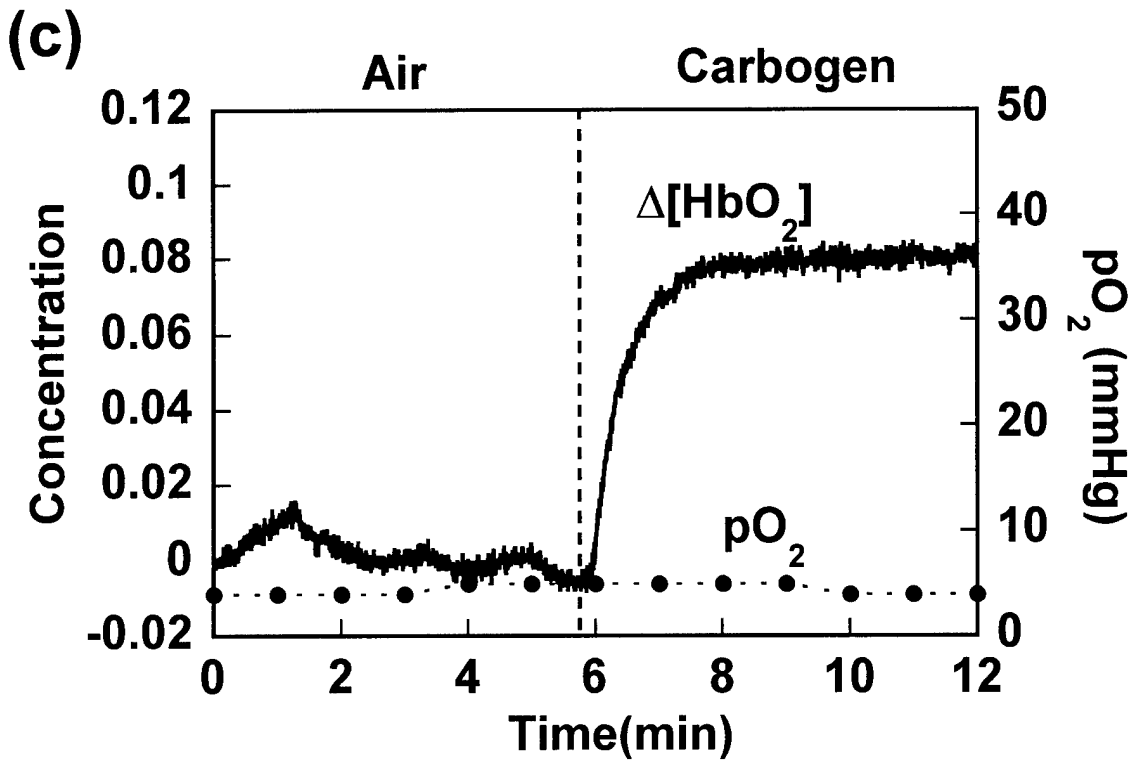
(c)
Air
Carbogen
0.12
0.1
0.08
0.06
0.04
0.02
0
-0.02
Concentration
50
40
30
20
10
0
pO2 (mmHg)
Δ[HbO2]
pO2
0
2
4
6
8
10
12
Time(min)

Figure 3

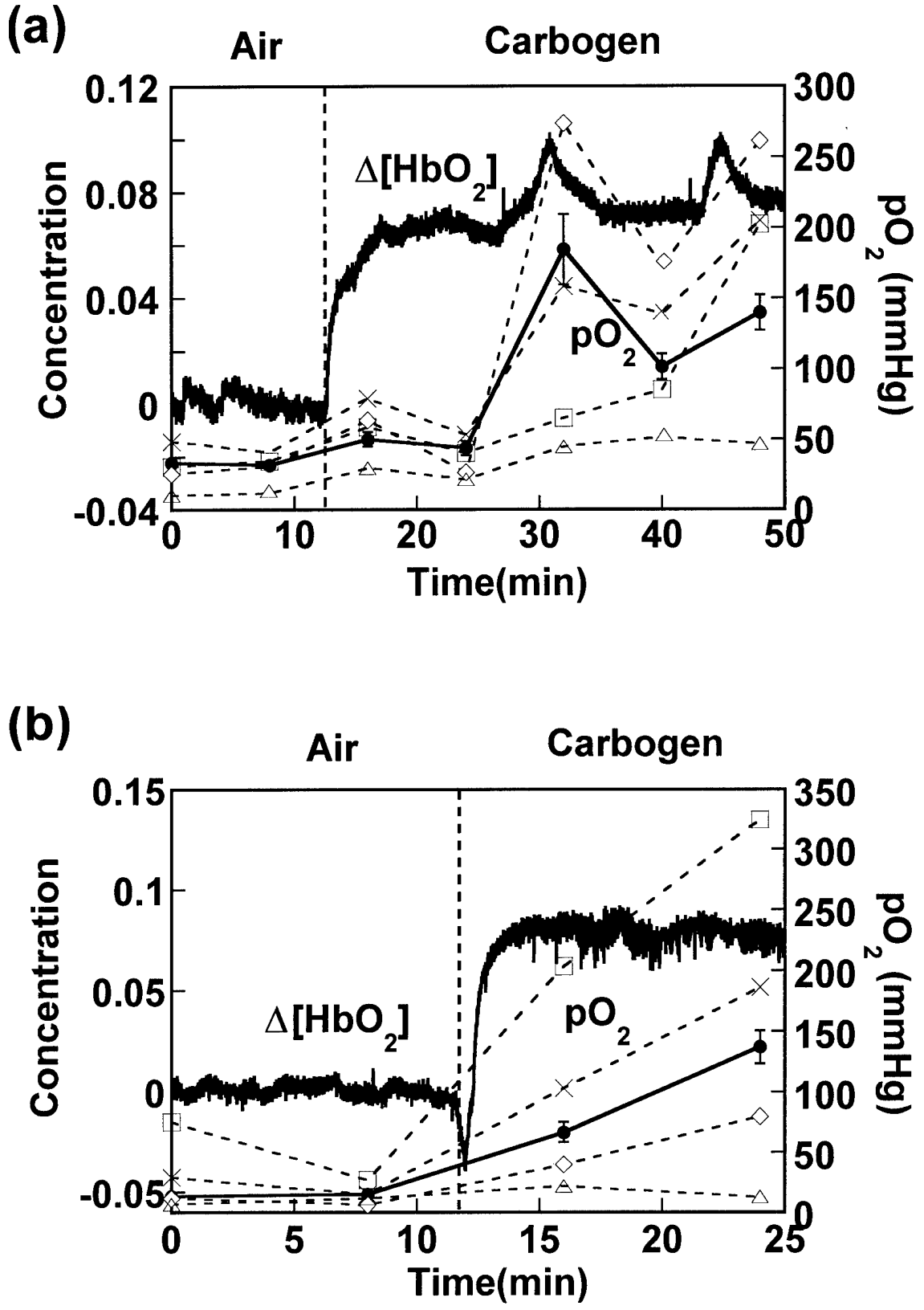
(a)
Air
Carbogen
0.12
0.08
0.04
0
-0.04
Concentration
Δ[HbO2]
pO2
300
250
200
150
100
50
0
pO2 (mmHg)
0
10
20
30
40
50
Time(min)
(b)
Air
Carbogen
0.15
0.1
0.05
0
-0.05
Concentration
Δ[HbO2]
pO2
350
300
250
200
150
100
50
0
pO2 (mmHg)
0
5
10
15
20
25
Time(min)

Figure 4

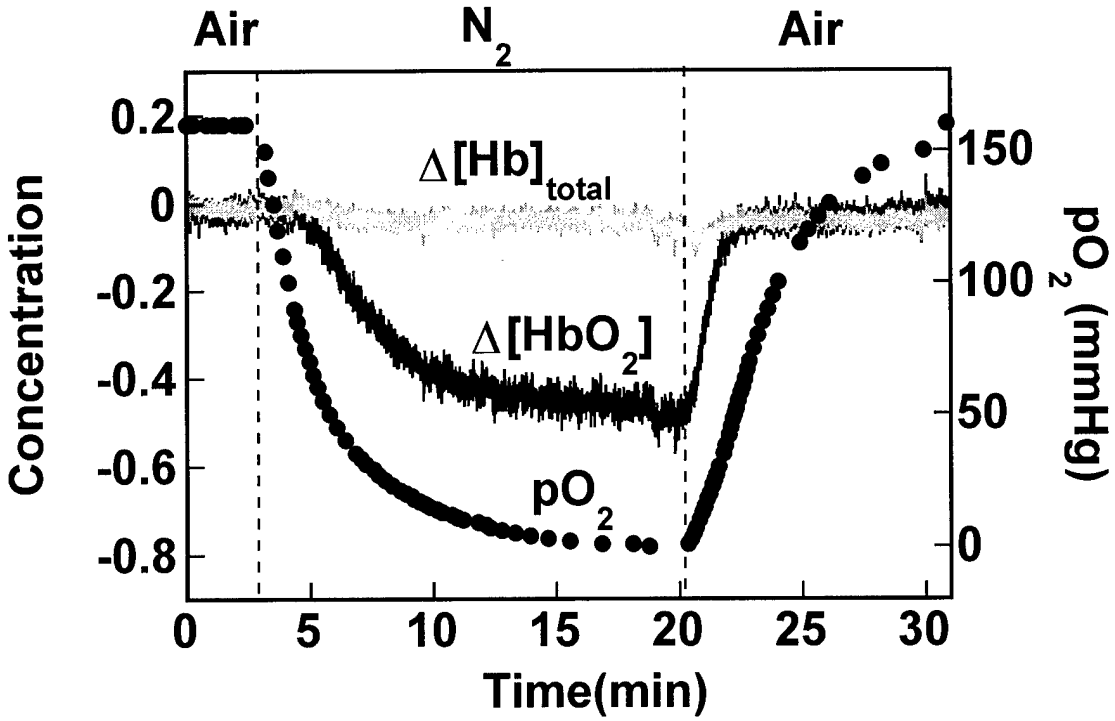
Air
N2
Air
0.2
0
-0.2
-0.4
-0.6
-0.8
Concentration
Δ[Hb]total
Δ[HbO2]
pO2
150
100
50
0
pO2 (mmHg)
0
5
10
15
20
25
30
Time(min)

Figure 5

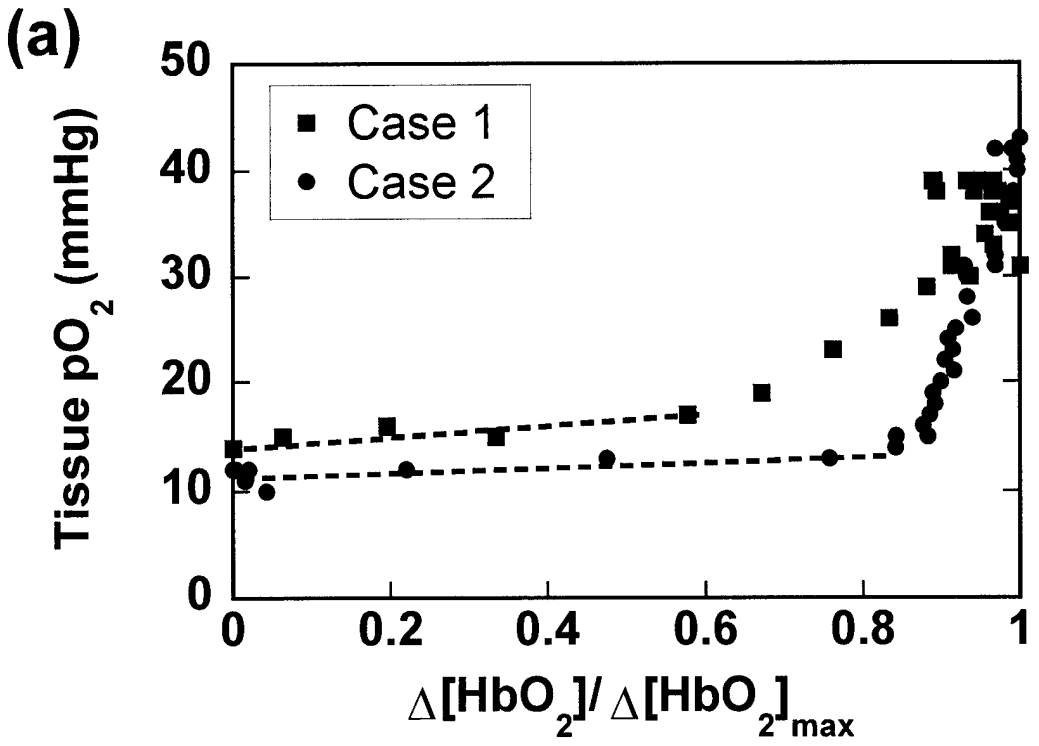
(a)
Tissue pO_2 (mmHg)
50
40
30
20
10
0
Case 1
Case 2
0
0.2
0.4
0.6
0.8
1
$\Delta[HbO_2]/\Delta[HbO_2]_{max}$

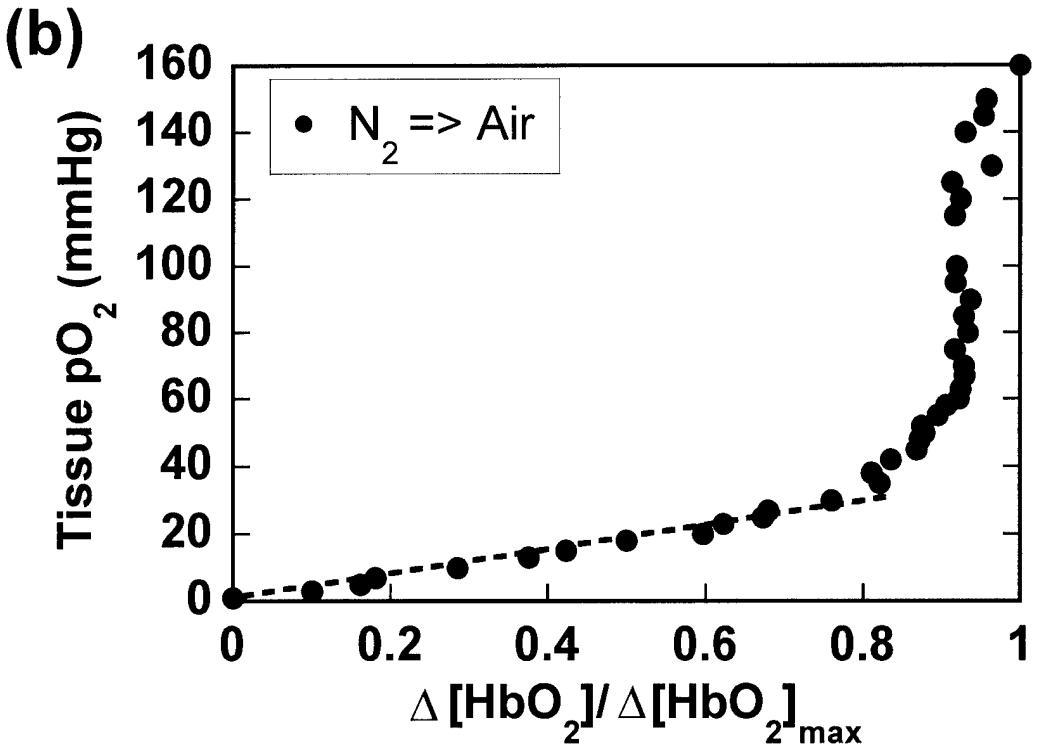
(b)
Tissue pO_2 (mmHg)
160
140
120
100
80
60
40
20
0
N_2 => Air
0
0.2
0.4
0.6
0.8
1
$\Delta[HbO_2]/\Delta[HbO_2]_{max}$

Figure 6

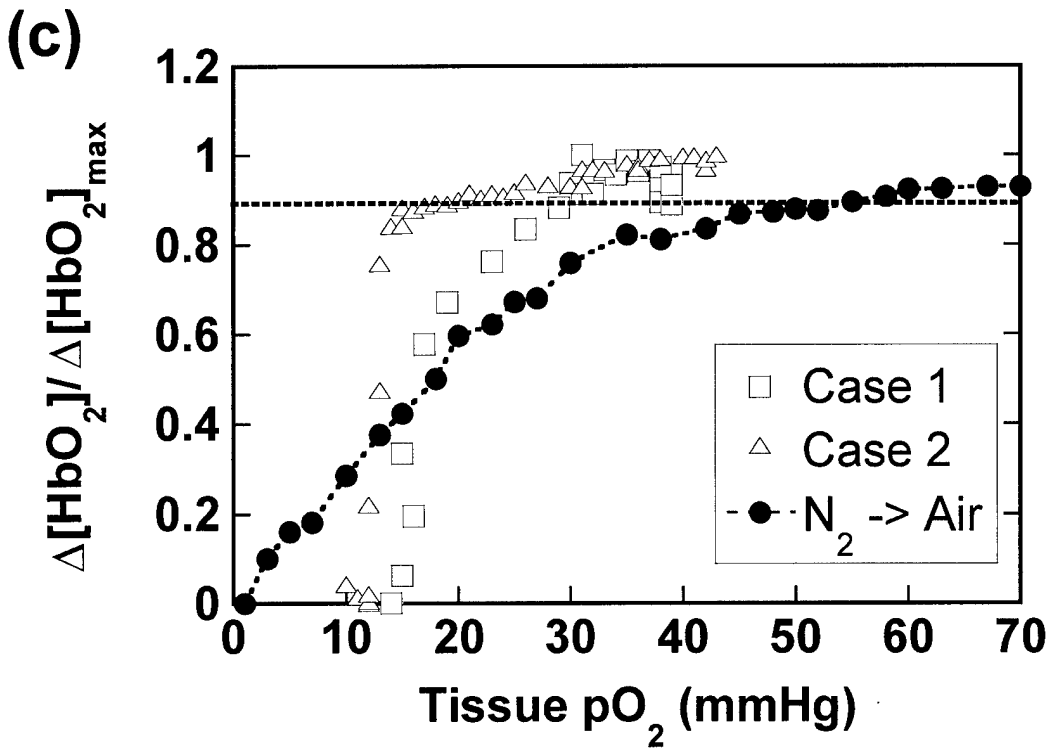
(c)
1.2
1
0.8
0.6
0.4
0.2
0
0
10
20
30
40
50
60
70
Δ[HbO2]/Δ[HbO2]max
Tissue pO2 (mmHg)
Case 1
Case 2
N2 -> Air

Figure 6

TUMOR OXYGENATION AND PHYSIOLOGY IN RESPONSE TO THERAPEUTIC INTERVENTIONS INVESTIGATED BY ^{19}F MRI AND NIR SPECTROSCOPY

By

Yulin Song

DISSERTATION

Presented to the Faculty of the Graduate Schools of

The University of Texas at Arlington and

The University of Texas Southwestern Medical Center at Dallas

In Partial Fulfillment of the Requirements

For the Degree of

DOCTOR OF PHILOSOPHY

The University of Texas Southwestern Medical Center at Dallas

Dallas, Texas

May 2001

TABLE OF CONTENTS